where prod = $\prod_{k=1}^{N} \hat{d}_{kk}$, $\omega(1,2)$ denotes the Coulombic interaction between electrons 1 and 2; and P_{12} is the usual permutation operator. If we adopt the standard chemist's notation for two-electron integrals, the last equation may be written as

$$\Omega_{AB}^{(2)} = \tfrac{1}{2}(\det \mathbf{U})(\det \mathbf{V}^{\dagger})(\mathrm{prod})^{-1} \sum_{\mu\nu\lambda\sigma}^{M} P_{\mu\nu}P_{\lambda\sigma}\{(\mu\nu|\lambda\sigma) - \langle\mu\sigma|\lambda\nu\rangle\} \quad \text{(A-8)}$$

Here $(\mu\nu|\lambda\sigma) = (\chi_\mu\chi_\lambda|\omega(1,2)|\chi_\nu\chi_\sigma\rangle$. Now let us specialize the above formulas for our particular case in which the molecular orbitals are either α spin or β spin. In this case the overlap matrix **D** is block diagonal and so are **V**, **U**, $\hat{\mathbf{d}}$, **A**, **B**, and **P**. As a result we have (from eq A-7)

$$\Omega_{AB}^{(1)} = (\det \mathbf{U})(\det \mathbf{V}^{\dagger})\{\sum_{\mu\nu}^{M} P_{\mu\nu}^{\alpha}\omega_{\mu\nu} + \sum_{\mu\nu}^{M} P_{\mu\nu}^{\beta}\omega_{\mu\nu}\}$$

or

$$\Omega_{AB}^{(1)} = (\det \mathbf{U})(\det \mathbf{V}^{\dagger})\sum_{\mu\nu}^{M} P_{\mu\nu}^{t}\omega_{\mu\nu} \quad \text{(A-9)}$$

where $\mathbf{P}^t = \mathbf{P}^\alpha + \mathbf{P}^\beta$. It is also assumed that the trivial spin integration in $\omega_{\mu\nu}$ is already performed.

Similarly, from eq A-8 we get

$$\Omega_{AB}^{(2)} = \tfrac{1}{2}(\det \mathbf{U})(\det \mathbf{V}^{\dagger}) \times (\mathrm{prod})^{-1}\{\sum_{\mu\nu\lambda\sigma}^{M} P_{\mu\nu}^{\alpha}P_{\lambda\sigma}^{\alpha}[(\mu\nu|\lambda\sigma) - (\mu\sigma|\lambda\nu)] + \sum_{\mu\nu\lambda\sigma}^{M} P_{\mu\nu}^{\alpha}P_{\lambda\sigma}^{\beta}(\mu\nu|\lambda\sigma) + \sum_{\mu\nu\lambda\sigma}^{M} P_{\mu\nu}^{\beta}P_{\lambda\sigma}^{\alpha}(\mu\nu|\lambda\sigma) + \sum_{\mu\nu\lambda\sigma}^{M} P_{\mu\nu}^{\beta}P_{\lambda\sigma}^{\beta}[(\mu\nu|\lambda\sigma) - (\mu\sigma|\lambda\nu)]\}$$

or after some simple manipulations we get

$$\Omega_{AB}^{(2)} = \tfrac{1}{2}(\det \mathbf{U})(\det \mathbf{V}^{\dagger}) \times (\mathrm{prod})^{-1} \sum_{\mu\nu\lambda\sigma}^{M} [P_{\mu\nu}^{t}P_{\lambda\sigma}^{t} - P_{\mu\nu}^{\alpha}P_{\lambda\sigma}^{\alpha} - P_{\mu\nu}^{\beta}P_{\lambda\sigma}^{\beta}](\mu\nu|\lambda\sigma) \quad \text{(A-10)}$$

Here $(\mu\nu|\lambda\sigma)$ is similar to $(\mu\nu|\lambda\sigma)$ except in the former the spin integration is already done. Note that eqs A-9 and A-10 bear a formal resemblance to that of standard one-electron and two-electron sums in LCAO-MO methods.

Our program module linked to the HONDO package consists of the following steps:

1. Carry out steps 2-5 below for both α- and β-occupied molecular orbitals.
2. Calculate the overlap matrix **D** from $\mathbf{D} = \mathbf{B}^{\dagger}\mathbf{S}\mathbf{A}$, where **A** and **B** are the eigenvectors of the diabatic states and **S** is the overlap matrix over atomic orbitals. The latter three matrices are part of standard output in LCAO-MO programs.
3. Perform the corresponding orbital transformation by computing the singular value decomposition of the real matrix **D** as $\mathbf{D} = \mathbf{U}\hat{\mathbf{d}}\mathbf{V}^{\dagger}$ and determine **U**, **V**, and the diagonal matrix $\hat{\mathbf{d}}$.
4. As an internal check, compute det **U** and det **V**. The absolute value of both quantities should be unity since **U** and **V** are unitary matrices.
5. Form matrices $\hat{\mathbf{A}}$ and $\hat{\mathbf{B}}$ as well as the diagonal matrix **T**, using $\hat{\mathbf{A}} = \mathbf{A}\mathbf{V}$, $\hat{\mathbf{B}} = \mathbf{B}\mathbf{U}$, and $T_{ii} = \prod_{j\neq i}^{N} \hat{d}_{jj}$. Then compute the generalized density matrix **P** by $\mathbf{P} = \hat{\mathbf{A}}\mathbf{T}\hat{\mathbf{B}}^{\dagger}$.
6. Compute S_{AB} from (eq 21 of ref 29)

$$S_{AB} = (\det \mathbf{U})(\det \mathbf{V}^{\dagger})(\mathrm{prod}) \quad \text{(A-11)}$$

7. Compute $\Omega_{AB}^{(1)}$ and $\Omega_{AB}^{(2)}$ by using eqs A-9 and A-10, respectively. Then compute H_{AB} by $H_{AB} = \Omega_{AB}^{(1)} + \Omega_{AB}^{(2)}$ and finally V_{AB} by using eq 2.

Dynamics of Ferrocene in a Thiourea Inclusion Matrix

Michael D. Lowery,[1] Richard J. Wittebort,*[,2] Michio Sorai,[3] and David N. Hendrickson*[,4]

Contribution from the Department of Chemistry, D-006, University of California at San Diego, La Jolla, California 92093-0506, Department of Chemistry, University of Louisville, Louisville, Kentucky 40292, School of Chemical Sciences, University of Illinois, Urbana, Illinois 61801, and Chemical Thermodynamics Laboratory, Faculty of Science, Osaka University, Toyonaka, Osaka 560, Japan. *Received May 30, 1989*

Abstract: ^{57}Fe Mössbauer and solid-state ^{2}H NMR spectroscopy are used to investigate the orientation and onset of motion of $Fe(C_5D_5)_2$ in the channels of the thiourea inclusion compound. ^{2}H NMR spectra obtained by rotating a single crystal of $Fe(C_5D_5)_2{\cdot}3(NH_2)_2CS$ about two orthogonal axes have been simulated and indicate that there are six different static ferrocene orientations at 140 K. At 140 K ~55% of the ferrocenes are located in three positions related by the crystallographic C_3 axis, where the ferrocene molecular axis is perpendicular to the channel axis of the thiourea host. The other three static ferrocene positions, which are interrelated by the C_3 axis, are located with the ferrocene molecular axis ~17° off the C_3 axis. In each of the perpendicular and parallel sites there is a distribution of ferrocene sites due to static disorder. Abruptly at the 160 K phase transition the perpendicular ferrocenes start jumping between the three perpendicular sites and the others start jumping between the three essentially parallel sites. Simulations of the Mössbauer spectra show that in the 160–225 K range the rate of interconversion of ferrocenes between perpendicular and parallel orientations is slower than ~10^5 s^{-1}. The Mössbauer spectrum changes from two doublets in the 160–220 K region to become one doublet and then a single Lorentzian peak in the 220–300 K range. Spectra for a single crystal show that the ^{2}H NMR spectrum collapses to a single doublet with a splitting of only 4.0 kHz with the field along the C_3 axis. A model is proposed that accounts not only for the spectroscopic observables but also for the heat capacity results, which show an entropy gain of $\Delta S \cong R \ln 4$ at the 160 K transition and little entropy gain in the 180–300 K range where the Mössbauer and ^{2}H NMR spectra change.

Since the accidental discovery by Bengen and Schlenk[5] that urea forms an inclusion compound with octal alcohol, urea and thiourea inclusion compounds have received considerable attention and are still the focus of active interest.[6] For example, Tam et

(1) University of Illinois.

(2) University of Louisville.

0002-7863/90/1512-4214$02.50/0

al.[7] very recently reported that organometallic complexes in thiourea inclusion matrices exhibit second harmonic generation (SHG) from 1.06-μm laser light. Inclusion in the channels of the thiourea host gives the acentric crystal structure required to give this non-linear effect. In this sense it is important to know whether a given organometallic complex is static or dynamic in the channels of the inclusion matrix, for a dynamic complex may not exhibit SHG.

In 1974, Clement et al.[8] first reported that ferrocene forms an inclusion compound with thiourea with a guest:host ratio of 1:3. They also noted from an X-ray rotating-crystal pattern that the ferrocene–thiourea compound was structurally similar (rhombohedral unit cell) to the cyclohexane–thiourea[9] inclusion compound. The ferrocene–thiourea inclusion compound exhibits an apparently first-order phase transition at $\sim$162 K as determined by DTA.[8] The observations of Clement et al.[8] were confirmed by others.[10,11]

Gibb[12] reported in 1976 the temperature dependence of the ^{57}Fe Mössbauer spectrum of the ferrocene–thiourea inclusion compound. The onset of motion of the ferrocene in the channels leads to averaging of the electric field gradient tensor. At temperatures less than $\sim$140 K all the ferrocene molecules were found to be "frozen" (i.e., static on the ^{57}Fe Mössbauer time scale of $\sim 10^{-7}$ s) in their lattice sites, with half of the ferrocene molecules oriented parallel to the thiourea channel axis and the remainder perpendicular to the channel axis. Upon increasing the temperature above $\sim$140 K the Mössbauer spectrum changes from one doublet to two. The new doublet was attributed to ferrocene molecules that are perpendicular to the channel axis (*c* axis), becoming dynamic in the *ab* plane. By theoretically modeling the temperature-dependent Mössbauer spectrum Gibb concluded that above $\sim$210 K ferrocene molecules not only are dynamic in the *ab* plane but there is an increasing rate of exchange of molecules between the perpendicular and parallel directions. Above $\sim$300 K only a single Lorentzian line shape is present, for the ferrocene molecules are tumbling rapidly between all positions.

In 1978 Hough and Nicholson[13] reported the results of a detailed X-ray crystallographic study of the ferrocene–thiourea inclusion compound at 295 and 100 K. At 295 K the crystals are rhombohedral ($R\bar{3}c$ with $Z = 6$). The space group $R\bar{3}c$ implies either $\bar{3}$ or 32 point symmetry for the six iron atoms and 2-fold symmetry for the 18 thiourea molecules in the unit cell. It was concluded that at 295 K either the molecular axis of the ferrocene molecule lies perpendicular to the channel axis or the molecular axis is inclined at various angles less than 90° relative to the channel axis. It was also possible that there was some combination of the above two situations. It was concluded that it is not likely to have two nearest neighbor ferrocene molecules with their molecular axes parallel to the channel axis, for this requires the cyclopentadienyl rings of the two molecules to be only 2.88 Å apart. Unfortunately, Hough and Nicholson found that below the $\sim$160 K phase transition the crystal reversibly twins.

Sorai et al.[14] employed adiabatic calorimetry to determine accurate heat capacity data for the thiourea inclusion compounds with either $Fe(C_5H_5)_2$[14a] or $Fe(C_5D_5)_2$.[14b] Five distinct thermal anomalies were detected at 219.0, 187.1, 173.4, 160.6, and 145.8 K, which were designated as the critical temperatures T_{C1}, T_{C2}, T_{C3}, T_{C4}, and T_{C5}, respectively. The thermal effect at 160.6 K (T_{C4}) has by far the largest enthalpy change. The abruptness of entropy gain and hysteresis seen for the 160.6 K thermal effect strongly suggests that this peak corresponds to a first-order phase transition. The transition entropy gain was found[14a] to be 9.23 J/(mol K) at T_{C4} and 1.79 J/(mol K) at T_{C5} for the $Fe(C_5H_5)_2$ inclusion compound. The total entropy change for the five phase transitions was found to be 11.52 J/(mol K) for thiourea with $Fe(C_5D_5)_2$ and 11.65 J/(mol K) with $Fe(C_5H_5)_2$. These values are close to R ln 4 (=11.53 J/(mol K)).

The goals of the present work are the following: (1) to study with ^{2}H NMR employing single-crystal and powder samples the dynamics of both the guest, $Fe(C_5D_5)_2$, and host, $(ND_2)_2CS$; (2) to use ^{2}H NMR to see whether onset of motion of the thiourea lattice occurs at the phase transitions; (3) to obtain ^{57}Fe Mössbauer spectra with a signal-to-noise improved from what Gibb[12] reported; and (4) to develop a model for the onset of molecular motion that would account for the spectroscopic as well as thermodynamic data. We note that the two techniques used here are complementary in that the dynamical averaging of an electric quadrupole moment is studied and the underlying exchange theory is equivalent. Dynamics slow compared to the quadrupole couplings ($\sim 10^5$ s^{-1} for ^{2}H NMR and $\sim 10^7$ s^{-1} for ^{57}Fe Mössbauer spectroscopy) appear as stationary, dynamics fast compared to the couplings lead to reduced equilibrium averages of the couplings, and rates comparable to the couplings give line-broadening effects. In the course of this study Clayden et al.[15] briefly reported ^{2}H NMR data for a powder sample of ferrocene($-d_{10}$)–thiourea inclusion compound. They concluded that the ferrocene molecules reorient rapidly above $\sim$300 K in a nearly isotropic fashion.

Experimental Section

Sample Preparation. A sample of the ferrocene($-d_{10}$)–thiourea inclusion compound was prepared with use of ethanol as the solvent as before.[14] The isotopic purity of the sample was determined to be greater than 99.8%. Ferrocene–thiourea($-d_4$) was prepared by using the method of Clement et al.[8] with the exception that C_2H_5OD was used as solvent.[14a] Thiourea-d_4 was prepared from thiourea by successive recrystallizations (four times) from 99% D_2O. Crystals suitable for the single-crystal ^{2}H NMR and ^{57}Fe Mössbauer experiments were obtained by slowly cooling a saturated solution of the clathrate in C_2H_5OD.

Instrumentation. ^{57}Fe Mössbauer measurements were made with use of a constant-acceleration-type instrument that has been described previously.[16] We estimate the absolute temperature accuracy to be $\pm$3 K; the relative precision is $\pm$0.5 K. Mössbauer spectra were least-squares fit to Lorentzian line shapes with a modified version of a previously documented computer program.[17] It should be noted that the isomer shifts illustrated in the figures are plotted as experimentally obtained and the tables should be consulted for corrected values.

^{2}H NMR experiments were performed on a "homebuilt" 5.9 T spectrometer described elsewhere.[18] The pulse sequence used was a standard quadrupole echo, [(90)$_x$–τ–(90)$_y$–τ–observe], with a delay time τ = 35 μs. ^{2}H NMR samples were $\sim$50 mg of powdered sample sealed in a Delrin tube ($^1/_4 \times {}^1/_2$ in.). In the case of the single-crystal work, crystals ($\sim$2 mm long, $\sim$0.25 mm wide) were expoxied onto Delrin holders that could be rotated about an axis perpendicular to the magnetic field. Crystals were mounted by eye with the needle axis of the crystals either

(3) Osaka University.
(4) University of California at San Diego.
(5) (a) Bengen, M. F.; Schlenk, W. *Experientia* **1949**, *5*, 200. (b) Bengen, M. F. *Angew. Chem.* **1953**, *63*, 207. (c) Schlenk, W. *Justus Liebigs Ann. Chem.* **1949**, *565*, 204.
(6) (a) Hagan, S. M. M. *Clathrate Inclusion Compounds*; Reinhold Publishing Corp.: New York, 1962. (b) Ferrely, L. C. *Non-Stoichiometry Compounds*; Mandelcorn, L., Ed.; Academic Press: New York, 1964; Chapter 8, pp 491–567. (c) *Inclusion Compounds*; Atwood, J. L., Davies, J. E. D., MacNicol, D. D., Eds.; Academic Press: New York, 1984; Volumes I–III. (d) For references specific to urea, thiourea, and seleourea see: Takemoto, K.; Sonoda, N. In *Inclusion Compounds*; Atwood, J. L., Davies, J. E. D., MacNicol, D. D., Eds.; Academic Press: New York, 1984; Chapter 2, Volume II.
(7) Tam, W.; Eaton, D. F.; Calabrese, J. C.; Williams, I. D.; Wang, Y.; Anderson, A. G. *Chem. Mater.* **1989**, *1*, 128–140.
(8) Clement, R.; Claude, R.; Mazieres, C. *J. Chem. Soc., Chem. Commun.* **1974**, 654.
(9) (a) Lenne, H. V. *Acta Crystallogr.* **1954**, *7*, 1. (b) Schlenk, W., Jr. *Annalen* **1951**, *573*, 142.
(10) Boazak, R. E.; Barone, A. D. *Chem. Lett.* **1975**, 75–76.
(11) (a) Nesmeyanov, A. N.; Shul'pin, G. B.; Rybinskaya, M. I. *Dokl. Akad. Nauk SSR* **1975**, *221(3)*, 624–626.
(12) Gibb, T. C. *J. Phys. C: Solid State Phys.* **1976**, *9*, 2627–2642.
(13) Hough, E.; Nicholson, D. G. *J. Chem. Soc. Dalton* **1978**, 15–18.
(14) (a) Sorai, M.; Shiomi, Y. *Thermochim. Acta* **1986**, *109*, 29–44. (b) Sorai, M.; Ogasahara, K.; Suga, H. *Mol. Cryst. Liq. Cryst.* **1981**, *73*, 231–254.
(15) Clayden, J. J.; Dobson, C. M.; Heyes, S. J.; Wiseman, P. J. *J. Incl. Phenom.* **1987**, *5*, 65–68.
(16) (a) Cohn, M. J.; Timken, M. D.; Hendrickson, D. N. *J. Am. Chem. Soc.* **1984**, *106*, 6683. (b) Federer, W. D. Ph.D. Dissertation, University of Illinois, 1984.
(17) Chrisman, B. L.; Tumolillo, T. A. *Comput. Phys. Commun.* **1971**, *2*, 322.
(18) (a) Wittebort, R. J.; Subramanian, R.; Kulshreshtha, N. P.; DuPre, D. B. *J. Chem. Phys.* **1985**, *83*, 2457. (b) Wittebort, R. J.; Woehler, S. E.; Bradley, C. H. *J. Magn. Reson.* **1986**, *67*, 143–148.

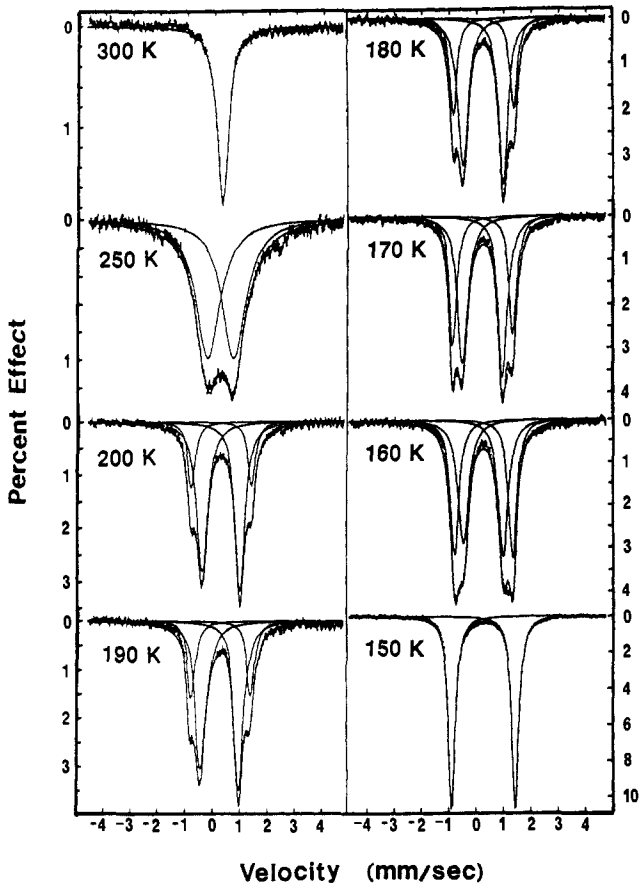

Figure 1. Variable-temperature ^{57}Fe Mössbauer spectra of a polycrystalline sample of the inclusion compound $Fe(C_5D_5)_2 \cdot 3(NH_2)_2CS$. The solid lines result from a least-squares fit of the data to Lorentzian line shapes.

parallel or perpendicular to the rotation axis. The material crystallizes as hollow hexagonal needles with crystal morphology directly reflecting the atomic structure.

Results and Discussion

^{57}Fe Mössbauer Results. Mössbauer spectra were run at 11 different temperatures in the range of 115–300 K for a polycrystalline sample of $Fe(C_5D_5)_2 \cdot 3(NH_2)_2CS$. Representative spectra are shown in Figure 1. Parameters obtained from a least-squares fit of the spectra to Lorentzian line shapes are summarized in Table I. The 115 K spectrum is comprised of one doublet with a quadrupole splitting (ΔE_Q) of 2.379 (1) mm/s and an isomer shift (δ) of 0.515 (1) mm/s vs iron foil at room temperature. These values compare well with those obtained at 87 K by Gibb:[12] ΔE_Q = 2.382 (2) mm/s and δ = 0.518 (2) mm/s. For polycrystalline ferrocene at 87 K, the single doublet is characterized[19] by ΔE_Q = 2.381 mm/s and δ = 0.520 mm/s. It is clear that the electric field gradient tensor is predominantly molecular in origin with little lattice contribution.

Gibb[12] reported the appearance of a new doublet at ~140 K when the compound was heated. However, with our samples and improved signal-to-noise spectra we do not see the appearance of a second doublet until ~160 K. The least-squares fitting parameters for this new "inner" doublet are ΔE_Q = 1.462 (9) mm/s and δ = 0.498 (4) mm/s with an average full-width at half-maximum (Γ) of 0.449 (1) mm/s. The area of this "inner" doublet at 160 K comprises ~54% of the total spectral area. The average line width of the 160 K "outer" doublet is 0.365 (1) mm/s, which is only slightly larger than is seen at 150 K (see Table I).

It should be noted that our sample of the ferrocene–thiourea inclusion compound was prepared with ethanol as the solvent. In the heat capacity study[14] it was found that ethanol gave a compound free of excess ferrocene, whereas employing methanol as a solvent gave, in our hands, a compound with excess ferrocene. Gibb[12] used methanol as a solvent. In fact, he noted that his room temperature ^{57}Fe Mössbauer spectrum had a weak signal with fitting parameters very similar to those of "static" ferrocene. In the case of phase transitions impurities can have pronounced effects on the temperature at which changes appear to happen. Gibb[12] attributed the "inner" doublet to ferrocene molecules that have their molecular axes reorienting rapidly in the *ab* plane (i.e., the plane perpendicular to the channel axis) and the "outer" doublet to static ferrocenes that have their molecular axes aligned with the *c* axis (i.e., collinear with the channel axis). Thus, abruptly at the 160.6 K first-order phase transition detected by adiabatic calorimetry[14] for $Fe(C_5H_5)_2 \cdot 3(NH_2)_2CS$ the ferrocenes oriented perpendicular to the channel axis become dynamic. Definitive support for this with important refinement and elaboration is given below.

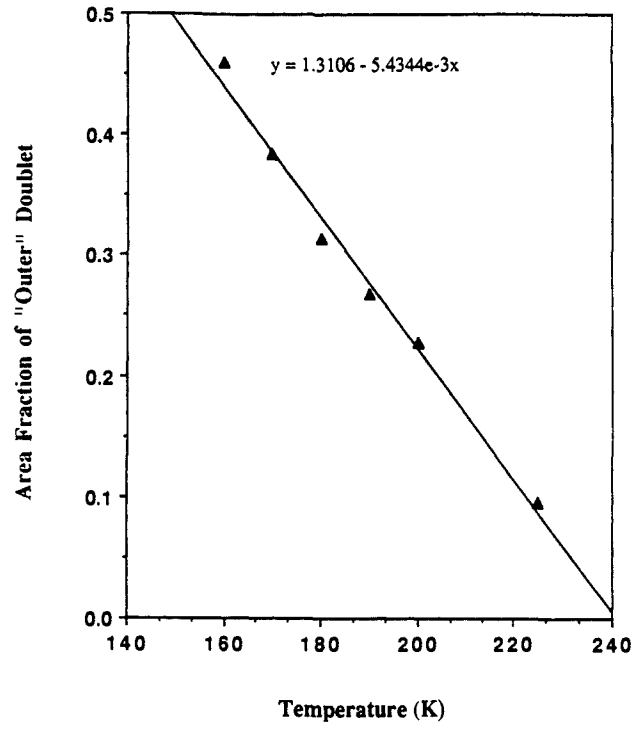

Figure 2. Plot of the area fraction of the outer quadrupole-split doublet versus temperature in the Mössbauer spectrum of a polycrystalline sample of $Fe(C_5D_5)_2 \cdot 3(NH_2)_2CS$. The outer doublet corresponds to those ferrocene molecules that are static. The data were least-squares fit to a straight line (shown).

An increase of the sample temperature above 160 K results in the inner doublet gaining intensity at the expense of the outer doublet (Figure 1). The area fraction of the outer doublet as a function of temperature in the range of 160–225 K is plotted in Figure 2 and is seen to decrease linearly with increasing temperature at a rate of 0.5% per degree. That the areas of these two doublets can be used to assess relative fractions of static and dynamic molecules is substantiated by the data in Figure 3. A plot of the natural logarithm of the background normalized total spectral area versus temperature is shown in Figure 3. Since there is no discontinuity or appreciable change evident, the vibrational nature of the solid is changing very little. Thus, there is little evidence for a change in recoilless fractions between static and dynamic molecules. Furthermore, in the 160–200 K range the line widths associated with the inner and outer doublets do not change appreciably. It is clear that throughout this range the rate of interconversion of ferrocene molecules between perpendicular and parallel orientations is slow ($<10^5$ s^{-1}) since they are represented by resolved doublets.

The 225 K Mössbauer spectrum of the polycrystalline sample of $Fe(C_5D_5)_2 \cdot 3(NH_2)_2CS$ was fit with two doublets. In contrast to the 160–200 K spectra, the line widths associated with the inner

(19) Gibb, T. C. *J. Chem. Soc. Dalton* **1976**, 1237 and references therein.

Table I. Mössbauer Fitting Parameters for the Polycrystalline Sample of $Fe(C_5D_5)_2 \cdot 3(NH_2)_2CS$[a]

temp, K	δ,[b] mm/s	ΔE_Q, mm/s	Γ,[c] mm/s	area[d] fraction	area[d] (normalized)	ln (area)
115	0.515 (1)	2.3787 (1)	0.298 (2)	0.500 (2)	3.511 (15)	1.256 (4)
			0.302 (2)	0.500 (2)		
150	0.506 (1)	2.3255 (10)	0.298 (2)	0.500 (2)	2.717 (11)	1.000 (4)
			0.296 (2)	0.500 (2)		
160	0.509 (3)	2.122 (6)	0.370 (10)	0.231 (1)	2.167 (13)	0.773 (6)
	0.498 (4)	1.462 (9)	0.472 (10)	0.269 (2)		
			0.426 (10)	0.269 (2)		
			0.360 (10)	0.231 (1)		
170	0.508 (3)	2.203 (5)	0.316 (9)	0.192 (1)	2.058 (12)	0.722 (5)
	0.502 (3)	1.485 (6)	0.444 (8)	0.308 (2)		
			0.404 (7)	0.308 (2)		
			0.346 (10)	0.192 (1)		
180	0.510 (3)	2.213 (6)	0.310 (10)	0.157 (1)	1.793 (10)	0.584 (6)
	0.494 (2)	1.481 (5)	0.466 (7)	0.343 (2)		
			0.398 (6)	0.343 (2)		
			0.328 (11)	0.157 (1)		
190	0.505 (3)	2.192 (6)	0.328 (11)	0.134 (1)	1.652 (9)	0.502 (5)
	0.491 (2)	1.405 (4)	0.464 (6)	0.366 (2)		
			0.406 (7)	0.366 (2)		
			0.338 (12)	0.134 (1)		
200	0.498 (3)	2.206 (6)	0.324 (10)	0.114 (1)	1.511 (7)	0.413 (4)
	0.483 (2)	1.387 (3)	0.484 (5)	0.386 (2)		
			0.426 (5)	0.386 (2)		
			0.332 (11)	0.114 (1)		
225	0.525 (11)	2.264 (22)	0.392 (37)	0.048 (1)	1.211 (6)	0.192 (5)
	0.482 (4)	1.295 (8)	0.758 (9)	0.452 (2)		
			0.678 (9)	0.452 (2)		
			0.456 (46)	0.048 (1)		
250	0.467 (3)	0.954 (6)	1.056 (15)	0.500 (4)	0.894 (7)	−0.112 (8)
			1.054 (14)	0.500 (4)		
275	0.492 (3)		0.922 (9)		0.589 (5)	−0.514 (8)
300	0.511 (2)		0.513 (6)		0.383 (3)	−0.960 (9)

[a] Parameters were obtained from a least-squares fit of the experimental data to Lorentzian line shapes. The data were fit with the constraint that the two components of a doublet were restricted to have equal areas. For each doublet, the parameters are listed in order of increasing velocity (down a column). [b] Isomer shifts are relative to magnetic iron foil at room temperature. [c] Full-width at half-maximum of the Lorentzian line shape. [d] Relative background normalized area of the total spectrum obtained from the least-squares fit.

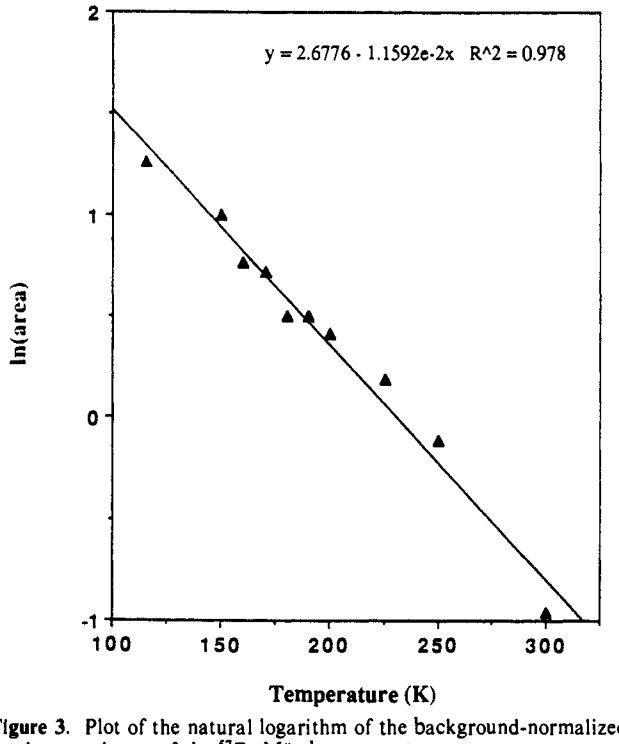

Figure 3. Plot of the natural logarithm of the background-normalized total spectral area of the ^{57}Fe Mössbauer spectrum versus temperature for a polycrystalline sample of $Fe(C_5D_5)_2 \cdot 3(NH_2)_2CS$.

doublet have increased significantly (see Table I). Figure 1 shows that above ~225 K all ferrocene molecules experience rapid ($> \sim 10^8$ s^{-1}) reorientations and only a single, broad doublet with reduced splitting is observed. A further increase in the sample temperature causes the doublet to collapse, so that by ~300 K only a single Lorentzian line shape is necessary to fit the spectrum. A rapid and nearly isotropic reorientation of ferrocene molecules between parallel and perpendicular orientations is present at 300 K.

Gibb[12] reported Mössbauer spectra at two temperatures, 87 and 173 K, for a partially oriented sample. We examined a collection of a few single crystals of $Fe(C_5D_5)_2 \cdot 3(NH_2)_2CS$ carefully oriented in the Mössbauer cell with the needle axis normal to the X-ray direction. Spectra were collected at 21 temperatures in the range 110–300 K, some of which are illustrated in Figure 4. All spectra were least-squares fit to Lorentzian line shapes, and the resulting parameters are given in Table II. Qualitatively, the temperature dependence of the single-crystal spectrum is very similar to that observed for the powdered sample. From 110 to 155 K essentially one doublet is present and at ~160 K a second doublet with reduced quadrupole splitting appears. In the range 160–220 K the relative areas of the two doublets change such that an increase in temperature leads to an increase in the percentage of the inner doublet associated with the dynamic ferrocene molecules. As with the powder data in this region, the line widths of both doublets are nearly temperature independent. Above ~230 K, a single doublet is observed for which the splitting decreases with increasing temperature.

Because the ferrocene molecules have a specific orientation relative to the γ-rays, the two components of each quadrupole doublet are not of equal area. The ratio I_+/I_-, where I_+ is the area of the more positive velocity component of a doublet, is a function of the angle between the principal axis of the electric field gradient tensor (along the C_5 axis of ferrocene) and the γ-ray direction. Thus the inequivalence of the two components of each doublet in the 110–155 K range can be used as a measure of the relative populations of ferrocene molecules oriented with their principal axes collinear with or in a plane perpendicular to the channel axis. It has been shown[12] that for static ferrocene

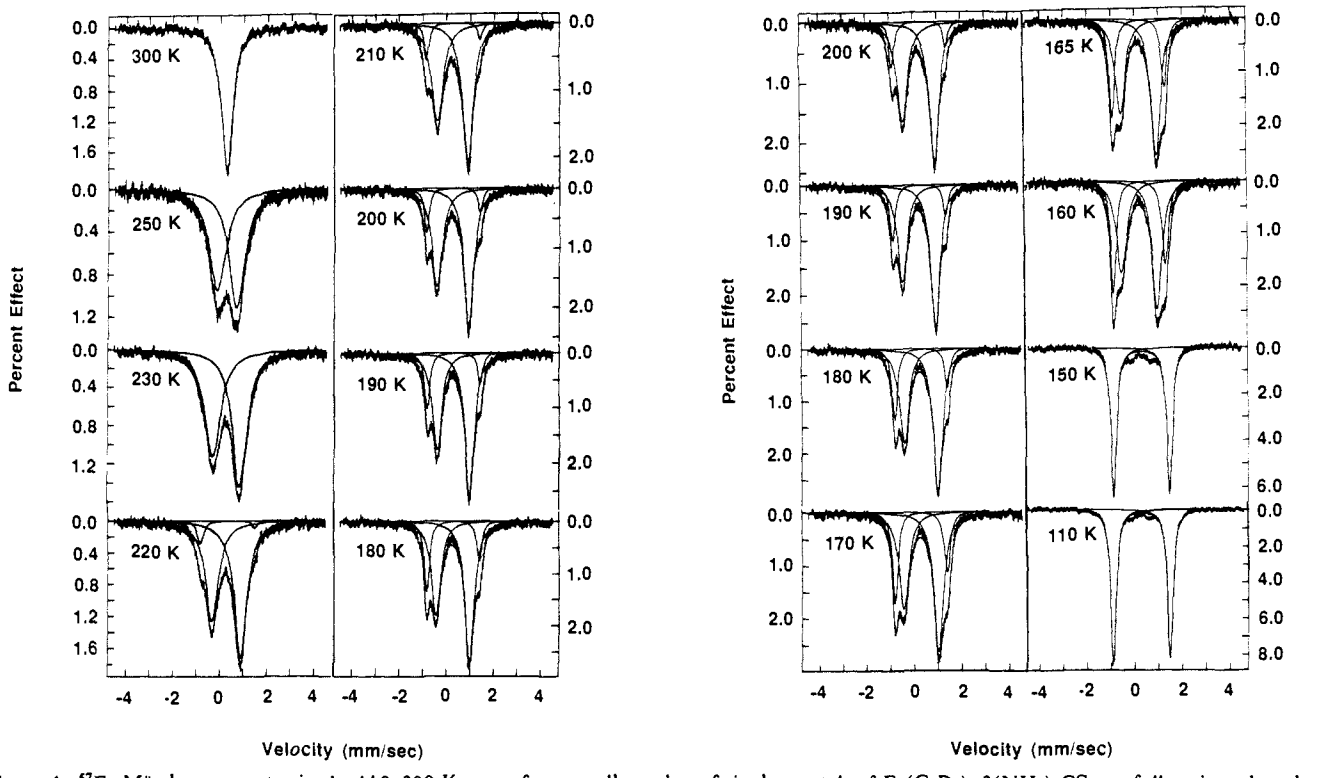

Figure 4. ^{57}Fe Mössbauer spectra in the 110–300 K range for a small number of single crystals of $Fe(C_5D_5)_2 \cdot 3(NH_2)_2CS$ carefully oriented so that the needle axis of the hexagonal crystals are oriented perpendicular to the γ-ray direction. Each spectrum was least-squares fit to Lorentzian line shapes.

molecules the ratio I_+/I_- is equal to 0.60 if the molecular axis is perpendicular to the γ-ray direction or 1.285 for ferrocene molecules randomly oriented in a plane parallel to the γ-ray direction. If we let p_z be the fraction of molecules with C_5 axes parallel to the channel axis and $p_\perp$ the fraction of molecules with C_5 axes in the *ab* plane, then $p_z + p_\perp = 1$ and the observed value of the ratio for the single doublet in the 110–155 K range is

$$(I_+/I_-)_{obs} = 0.600p_z + 1.285(1 - p_z) \qquad (1)$$

The values of I_+/I_- given in Table II were used to calculate p_z in the 110–155 K range and a plot of p_z versus temperature is shown in Figure 5. At 110 K 52% of the molecules are perpendicular to the channel axis and this fraction increases to ~60% at 155 K. In this plot is also shown the area fraction of the outer doublet for static ferrocenes in the 160–210 K range, which gauges the fraction of ferrocenes statically oriented parallel to the channel axis.

It was asserted above that at the first-order phase transition, 160.6 K, the ferrocene molecules in the *ab* plane become dynamic. This leads to the sudden appearance of the inner Mössbauer doublet at ~160 K. The fact that this doublet is associated with ferrocene molecules, which are dynamic in the *ab* plane, is substantiated by the I_+/I_- ratio for this doublet. In Table II it can be seen that this ratio is equal to 1.3 (2) in the 160–210 K range and thus is in agreement with the expected value of 1.285.

Figure 6 shows a plot of ΔE_Q versus temperature (110–250 K) for the oriented single-crystal sample of $Fe(C_5D_5)_2 \cdot 3(NH_2)_2CS$. If the ferrocene molecules were jumping rapidly on the Mössbauer time scale between two sites (or three sites related by 120°) with equal populations in each site in the *ab* plane, then ΔE_Q for the inner doublet should be one-half that for the outer doublet for the static molecules. To further clarify the assumption of slow parallel-to-perpendicular interconversion we simulated the powder Mössbauer spectra using the equations derived by Gibb[12] for a Mössbauer nucleus with an electric field gradient jumping randomly between three mutually orthogonal directions.

We have used the anisotropic *XY* exchange model[12] to simulate the spectra in the 160–200 K temperature range. This model assumes that there is *no* exchange between the parallel and perpendicular ferrocene sites and that the exchange rate between the perpendicular sites is anisotropic (i.e. $\tau_{xy} \neq \tau_{yx}$). The parameters used to simulate the spectra are given in Table III. The population fractions were determined independently from the ratio of the static to dynamic quadrupole splitting values; see ref 19 for details. The correlation times were then adjusted in an ad hoc fashion to obtain the best fit of the experimental spectra. Thus, only one independent variable (τ_{xy}) was needed to simulate the ^{57}Fe Mössbauer spectra between 160 and 200 K. The 250 and 300 K spectra were simulated by using the isotropic *XY* model

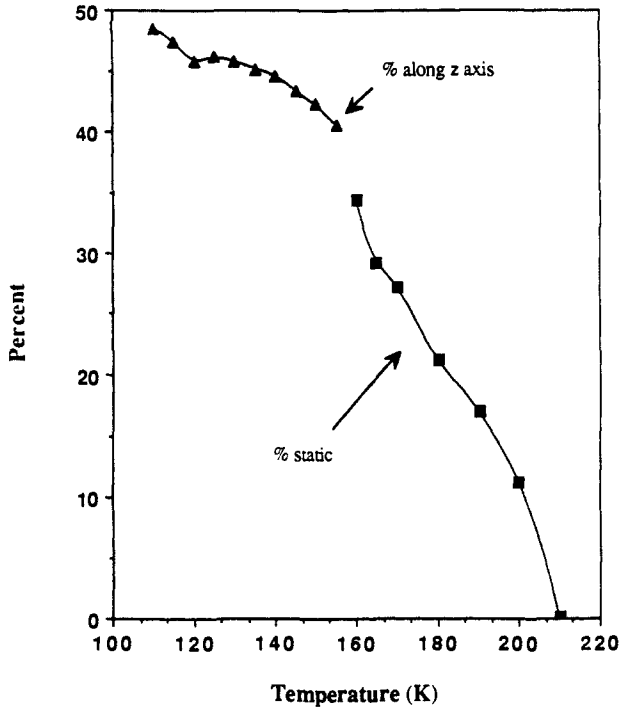

Figure 5. Plot of percent of ferrocenes oriented with their molecular axis collinear with the channel axis versus temperature for $Fe(C_5D_5)_2 \cdot 3(NH_2)_2CS$. In the 110–150 K range the evaluation of percentages came from Mössbauer data for a single-crystal sample. In the 160–210 K range the percent of parallel oriented ferrocenes was evaluated from Mössbauer spectra for a polycrystalline sample.

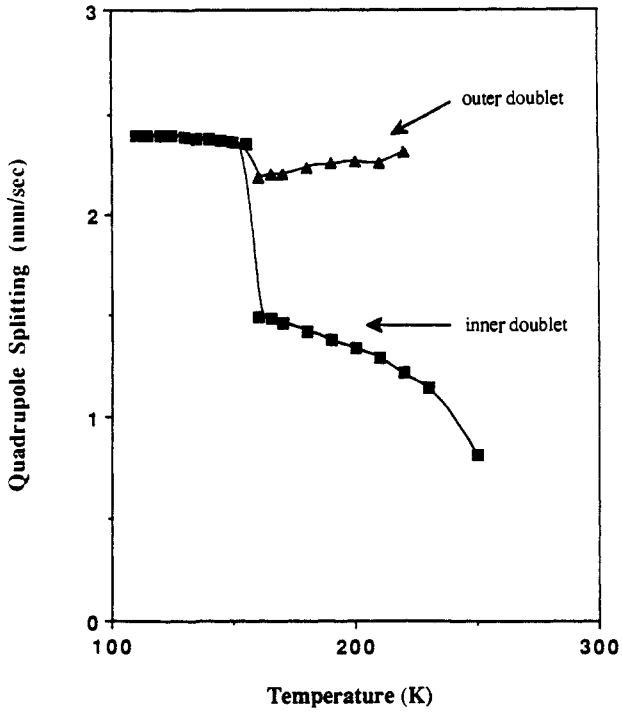

Figure 6. Temperature dependence of the quadrupole splitting for the inner and outer doublets observed in the ^{57}Fe Mössbauer spectrum obtained for a single-crystal sample of $Fe(C_5D_5)_2 \cdot 3(NH_2)_2CS$.

derived by Gibb.[12] When modeling these spectra, we have assumed that the exchange rate in the *ab* plane is in the fast exchange limit ($\tau_{xy} < 10^{-9}$ s) so that the line shape is controlled by exchange between parallel and perpendicular lattice sites. For these spectra, the correlation times were determined from the line width (Γ) of the experimental spectra,[12] and the population fractions were adjusted to fit the data. A Fortran program[19] was written to simulate the powder spectra according to the equations of Gibb.[12]

In Figure 7 are shown the best simulations of the experimental powder spectra with use of the parameters given in Table III. At 150 K the correlation time for motion in the *ab* plane is long ($\tau_{xy} > 10^{-4}$ s), as is the correlation time ($\tau_{xz} = \tau_{yz}$) for interconversions between orientations in the *ab* plane and the *c* axis. That is, all molecules are static on the ^{57}Fe Mössbauer time scale at 150 K. Above 160 K the rate of motion in the *ab* plane is fast (i.e., $\tau_{xy} < 10^{-8}$ s). It is important to note that in the 160–200 K range we had to keep $\tau_{xz} = \tau_{yz} = \sim 10^{-5}$ s. This corresponds to a slow rate of perpendicular-to-parallel interconversion relative to the Mössbauer time scale. A decrease in τ_{xz} (increase in exchange rate) leads to increased line widths. In the 160–200 K range only the population fractions p_z and $p_\perp$ and the anisotropic τ_{xy} exchange rate needed to be changed to fit the experimental spectra. Only in the case of the 250 and 300 K simulations was it necessary to decrease τ_{xz}. Thus, the simulations are consistent with slow *ab* plane to *c* axis interconversions in the 160–210 K range. It is interesting to note that, in the range of 160–210 K, ΔE_Q for the outer doublet is relatively constant. However, the value of ΔE_Q for the inner doublet decreases gradually from 1.499 (10) mm/s at 160 K to 1.295 (6) mm/s at 210 K. This and the fact that ΔE_Q for the inner doublet is larger than one-half of the ΔE_Q value for the outer doublet at each temperature strongly indicates that the motion in the *ab* plane has less than 3-fold symmetry. For example, at 160 K, ΔE_Q for the outer doublet is 2.183 (6) mm/s, whereas ΔE_Q for the inner doublet is 1.499 (10) mm/s. Even at 210 K the corresponding values are 2.257 (13) and 1.295 (6) mm/s, respectively.

^{2}H NMR Results. Variable-temperature deuterium magnetic resonance spectra were run for single-crystal or polycrystalline samples of either $Fe(C_5D_5)_2 \cdot 3(NH_2)_2CS$ or $Fe(C_5H_5)_2 \cdot 3(ND_2)_2CS$. The two different sites of deuteriation allow us to examine independently the orientations and possible dynamics of both the inclusion guest and host.

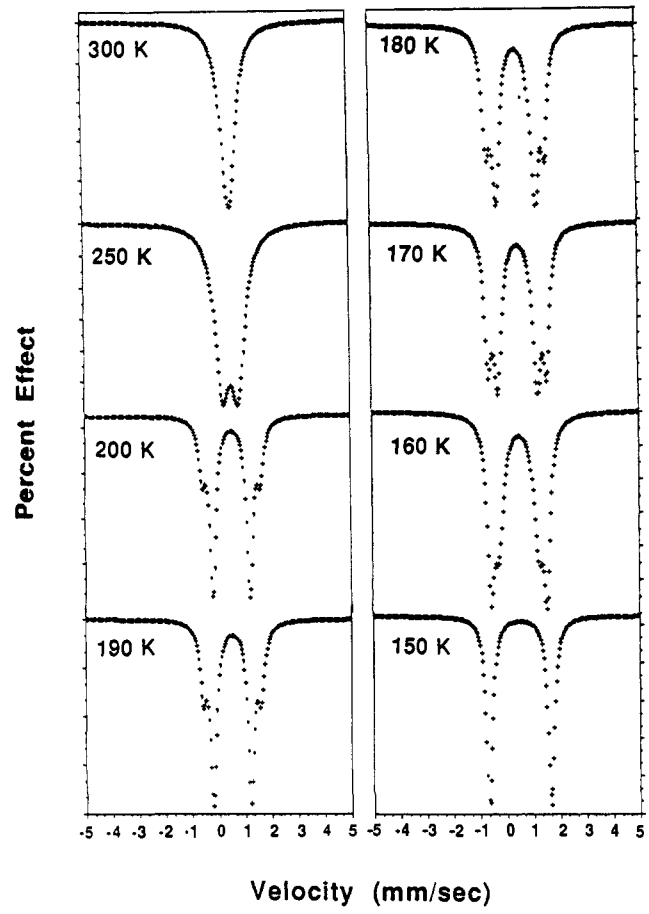

Figure 7. Simulated ^{57}Fe Mössbauer spectra for a powdered sample of $Fe(C_5D_5)_2 \cdot 3(NH_2)_2CS$. The spectra were generated with use of the parameters given in Table III. Spectra between 160 and 200 K were constructed by using the anisotropic *XY* model, while the higher temperature spectra were obtained by using the isotropic *XY* model. The value for the static quadrupole splitting value at each temperature (Δ_0) was assumed to be equal to the quadrupole splitting value for the outer quadrupole doublet and was taken from the experimental data presented in Table I. Additional parameters used in the simulation are $\delta = 0.506$ mm/s and $\Gamma = 0.30$, where these values were taken from a fit of the 150 K spectrum.

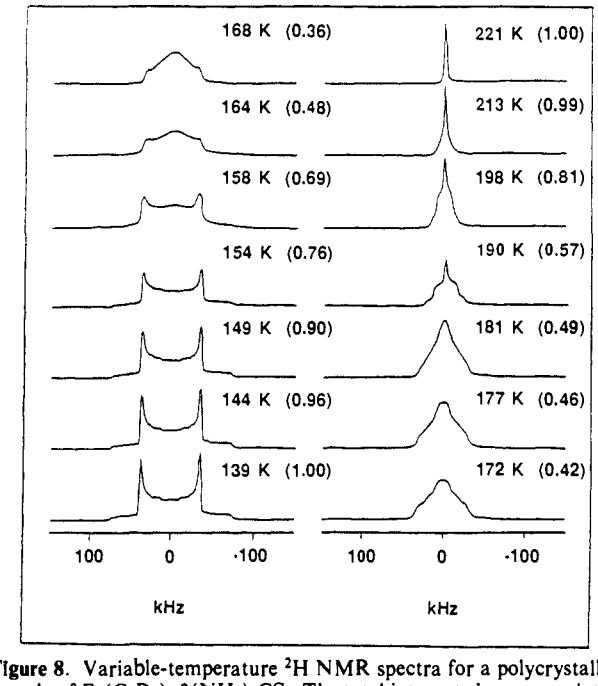

Figure 8. Variable-temperature ^{2}H NMR spectra for a polycrystalline sample of $Fe(C_5D_5)_2 \cdot 3(NH_2)_2CS$. The total integrated spectrum intensity is given in parentheses next to the temperature value.

Table II. Mössbauer Fitting Parameters for an Oriented Crystal Sample of $Fe(C_5D_5)_2 \cdot 3(NH_2)_2CS$[a]

temp, K	δ,[b] mm/s	ΔE_Q, mm/s	Γ,[c] mm/s	fractional area	area[d] (normalized)	ln (area)
110	0.515 (1)	2.3970 (13)	0.270 (3)	0.512 (3)	2.054 (12)	0.720 (5)
			0.270 (3)	0.488 (3)		
115	0.517 (1)	2.3960 (10)	0.272 (2)	0.510 (2)	2.796 (13)	1.028 (7)
			0.272 (2)	0.490 (2)		
120	0.513 (1)	2.3896 (15)	0.270 (3)	0.507 (3)	1.951 (13)	0.668 (6)
			0.274 (3)	0.493 (3)		
125	0.516 (1)	2.3962 (11)	0.276 (2)	0.508 (2)	2.657 (13)	0.977 (4)
			0.276 (2)	0.492 (2)		
130	0.512 (1)	2.3874 (15)	0.268 (3)	0.507 (3)	1.843 (12)	0.612 (6)
			0.266 (3)	0.493 (3)		
135	0.513 (1)	2.3772 (14)	0.268 (3)	0.506 (3)	1.781 (11)	0.577 (7)
			0.268 (3)	0.494 (3)		
140	0.513 (1)	2.3760 (17)	0.270 (4)	0.505 (4)	1.723 (13)	0.544 (8)
			0.270 (4)	0.495 (4)		
145	0.512 (1)	2.3682 (18)	0.274 (4)	0.503 (4)	1.677 (13)	0.517 (8)
			0.278 (4)	0.497 (4)		
150	0.510 (1)	2.3603 (23)	0.278 (5)	0.501 (5)	1.592 (16)	0.465 (9)
			0.284 (5)	0.499 (5)		
155	0.509 (1)	2.3492 (26)	0.286 (5)	0.498 (5)	1.505 (16)	0.408 (9)
			0.294 (5)	0.502 (5)		
160	0.500 (3)	2.183 (6)	0.264 (12)	0.180 (1)	1.420 (11)	0.350 (8)
	0.497 (5)	1.499 (10)	0.514 (21)	0.286 (2)		
			0.472 (14)	0.369 (3)		
			0.326 (18)	0.165 (1)		
165	0.504 (3)	2.198 (6)	0.274 (12)	0.167 (1)	1.362 (9)	0.309 (7)
	0.499 (4)	1.490 (8)	0.504 (17)	0.296 (2)		
			0.482 (12)	0.411 (3)		
			0.294 (17)	0.126 (1)		
170	0.502 (3)	2.198 (6)	0.268 (12)	0.156 (1)	0.308 (9)	0.269 (6)
	0.499 (3)	1.467 (7)	0.488 (16)	0.304 (2)		
			0.742 (11)	0.424 (3)		
			0.298 (19)	0.116 (1)		
180	0.516 (3)	2.235 (6)	0.266 (12)	0.136 (1)	1.197 (7)	0.180 (6)
	0.503 (3)	1.426 (5)	0.470 (12)	0.321 (2)		
			0.460 (8)	0.468 (3)		
			0.262 (20)	0.076 (1)		
190	0.519 (4)	2.253 (8)	0.266 (15)	0.111 (1)	1.094	0.090 (6)
	0.498 (2)	1.383 (5)	0.478 (12)	0.345 (2)		
			0.458 (8)	0.485 (3)		
			0.248 (23)	0.059 (1)		
200	0.520 (5)	2.264 (10)	0.236 (19)	0.079 (1)	1.011	0.011 (7)
	0.497 (3)	1.343 (5)	0.530 (15)	0.385 (3)		
			0.478 (9)	0.493 (4)		
			0.234 (32)	0.043 (1)		
210	0.525 (7)	2.257 (13)	0.238 (23)	0.060 (1)	0.971 (7)	−0.030 (7)
	0.494 (3)	1.295 (6)	0.598 (16)	0.403 (3)		
			0.530 (9)	0.510 (4)		
			0.224 (41)	0.027 (1)		
220	0.556 (16)	2.314 (32)	0.312 (52)	0.046*	0.900 (10)	−0.105 (11)
	0.494 (4)	1.217 (7)	0.660 (22)	0.415*		
			0.644 (13)	0.550*		
230	0.496 (2)	1.149 (5)	0.818 (14)	0.446 (3)	0.879 (5)	−0.129 (7)
			0.730 (10)	0.534 (4)		
250	0.500 (4)	0.820 (7)	0.840 (27)	0.474 (5)	0.750 (6)	−0.288 (11)
			0.792 (22)	0.526 (5)		
300	0.496 (2)		0.571 (6)		0.472 (4)	−0.751 (9)

[a] Parameters were obtained from a least-squares fit of the experimental data to Lorentzian line shapes. For each doublet, the parameters are listed in order of increasing velocity (down a column). Values marked with an "*" were too small to give accurate fitting parameters. [b] Isomer shifts are relative to magnetic iron foil at room temperature. [c] Full-width at half-maximum of the Lorentzian line shape. [d] Relative background normalized area of the total spectrum obtained from the least-squares fit.

Figure 8 shows quadrupole echo spectra obtained as a function of temperature for polycrystalline $Fe(C_5D_5)_2 \cdot 3(NH_2)_2CS$. Listed for each spectrum is the temperature and the total integrated spectral intensity corrected for the increased Boltzmann polarization as the temperature is lowered. Several useful qualitative results are immediately evident. For temperatures below 150 K, the powder pattern that is obtained is characteristic of a single residual quadrupole splitting, ν_q, of 73 kHz. This is just half the expected value for stationary aromatic deuterons and thus establishes that the cyclopentadienyl rings undergo rapid in-plane reorientation about local C_5 axes with no other dynamical disorder. Measurement of longitudinal relaxation times at 135 K shows substantial anisotropy with T_1 values of 17 and 80 ms for the parallel and perpendicular edges of the spectrum, respectively. This indicates a reorientation of cyclopentadienyl rings by 5-fold jumps with a correlation time of 70 ns.

For temperatures greater than 150 K, the spectral width decreases monotonically corresponding to an increased amplitude of reorientation of the ferrocene molecular axes as the temperature is increased. At 221 K, the pattern is approximately reduced to a sharp line and the ferrocene molecules are close to the limit of isotropic reorientation. Quantitative interpretation of the powder spectra at intermediate temperatures is difficult. Spectrum intensities, although equivalent at the high- and low-temperature limits, show a modest decrease at intermediate values with a minimum near 168 K (38%). The pattern shapes contain a sharp

Table III. Parameters Used To Simulate the Variable-Temperature ^{57}Fe Mössbauer Spectrum of a Powdered Sample of the Ferrocene($-d_{10}$)–Thiourea Inclusion Compound

temp, K	p_z[a]	p_x[b]	τ_{xz}[c]	τ_{xy}[d]
150	0.50	0.25	$>10^{-4}$	$>10^{-4}$
160	0.46	0.42	$\sim 10^{-5}$	2.5×10^{-8}
170	0.38	0.47	$\sim 10^{-5}$	5×10^{-8}
180	0.31	0.52	$\sim 10^{-5}$	5×10^{-8}
190	0.27	0.54	$\sim 10^{-5}$	5×10^{-8}
200	0.23	0.56	$\sim 10^{-5}$	5×10^{-8}
250	0.26	0.50	2×10^{-7}	$<10^{-9}$
300	0.30	0.35	7×10^{-8}	$<10^{-9}$

[a] Population fraction of ferrocene molecules oriented along the z axis (i.e. parallel to the channel axis). [b] Population fraction of ferrocene molecules oriented along the x axis (i.e. perpendicular to the channel axis). [c] Correlation time (in seconds) for exchange between the x and z axes. [d] Correlation time (in seconds) for exchange between the x and y axes.

central feature in addition to features at two other frequencies and thus do not indicate the presence of a single rapid motion-averaged residual powder pattern. In general the loss of signal intensity accompanying spectral narrowing in the quadrupole echo experiment suggests the onset of dynamical rates comparable to the coupling frequency. For example, it was found[20] in ^{2}H NMR studies of hexagonal ice where dueterons undergo high-symmetry tetrahedral reorientation with rates comparable to the quadrupole coupling that dramatic reductions in spectral intensity occur where the intensity decreases to a few percent of the high- and low-temperature limits. In the case of $Fe(C_5D_5)_2{\cdot}3(NH_2)_2CS$ we see only a modest intensity loss. This, together with the presence of well-defined spectral features, suggests that dynamical rates of reorientation of the molecular axis of ferrocene in thiourea are more than an order of magnitude smaller or larger than $\nu_q = 73$ kHz and that the ferrocene molecular axes do not all undergo equivalent dynamical averaging.

Figure 9 shows spectra obtained from $Fe(C_5H_5)_2{\cdot}3CS(ND_2)_2$. The powder patterns, which show quadrupole couplings, e^2qQ/h, of 204 kHz at 298 K, 208 kHz at 180 K, and 213 kHz at 140 K and a constant asymmetry of $\eta = 0.16$, are all close to that observed for the deuterons in solid urea and thus indicate that, aside from rapid small amplitude reorientations at the higher temperatures, the thiourea molecules forming the hexagonal channels are stationary from 140 to 298 K. Work by Clement et al.[21] and very recently work by Heaton, Vold, and Vold[22] show that in some urea inclusion compounds the urea molecules can undergo 180° flips about the carbonyl bonds. Such was not found to occur in the present study. This observation does not exclude lattice expansion at higher temperatures. Relaxation measurements show that T_1 varies from about 0.5 s at 298 K to 34 s at 140 K. Assuming, in accord with the very long relaxation time, that the ND_2 groups are static at low temperature, then the root-mean-square librational amplitude at the high temperature, 289 K, is readily estimated as

$$\theta_{rms} = \sqrt{\tfrac{2}{3}(1 - \nu_{q,obs}/\nu_{q,static})} \approx 10° \qquad (2)$$

Shown also in Figure 9 is the 289 K spectrum obtained from a single crystal with the crystallographic c axis, i.e., the channel axis, parallel to the magnetic field $\mathbf{H}_0$. For this orientation, independent of temperature and only this orientation, a single quadrupole doublet is observed with splitting just half that of the maximum observed for the powder patterns. For amide deuterons in urea and *N*-acetylglycine, single-crystal studies show that the

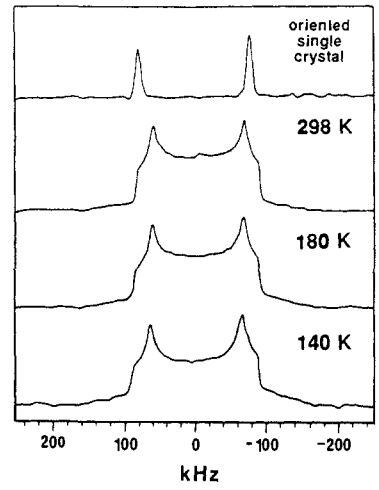

Figure 9. ^{2}H NMR spectra for a polycrystalline sample of $Fe(C_5H_5)_2{\cdot}3(ND_2)_2CS$. The powder patterns have quadrupole coupling values of 204 kHz at 289 K, 208 kHz at 180 K, and 213 kHz at 140 K. All of these powder spectra have the same asymmetry parameter of $\eta = 0.16$. In the top trace is given the 298 K ^{2}H NMR spectrum for a single crystal of $Fe(C_5H_5)_2{\cdot}3(ND_2)_2CS$ with the crystal needle axis parallel to the external magnetic field $\mathbf{H}_0$.

quadrupole coupling tensor has its largest component along the N–D bond. Thus, in the compound under study here, we can immediately conclude that the thiourea N–D bonds are all perpendicular to the channel axis. From the high-temperature X-ray structure, the C=S bond is perpendicular to the channel axis. Consequently, looking along the N–N axis of any thiourea molecule (or equivalently the channel axis) would show that for a given thiourea molecule the two ND_2 groups are in an eclipsed configuration and pointing in the opposite direction of the C=S bond. No other configuration allows all N–D bonds to be perpendicular to the channel axis.

Powder patterns of the ferrocene deuterated material in Figure 8 clearly show that for $T < 150$ K, ring dynamics are limited to strictly in-plane reorientations. Thus, the residual coupling tensor for all ten deuterons associated with a single ferrocene molecule is axially symmetric about the plane normal, i.e., collinear with the ferrocene molecular axis. In the ^{2}H NMR experiment each ferrocene molecule gives rise to a single quadrupole doublet with a splitting $\Delta\nu_q$ given by

$$\Delta\nu_q = \nu_q(3\cos^2\Omega - 1) \text{ and } \nu_q = 73 \text{ kHz} \qquad (3)$$

where Ω is the angle between the molecular axis and the magnetic field. Consequently, single-crystal ^{2}H NMR studies of $Fe(C_5D_5)_2{\cdot}3(NH_2)_2CS$ should be a good method for determining the molecular orientation(s) in the low-temperature solid phase, a problem unsolved by X-ray diffraction experiments.[13]

Shown in Figure 10 are a series of spectra obtained at 140 K. A single crystal with perdeuterated ferrocene was mounted with the c axis (channel direction) perpendicular to $\mathbf{H}_0$, and subsequently rotated through a series of angles, ϕ, about that axis. Crystals were mounted by visual inspection and thus angles have an absolute uncertainty of about 4° in this work. Spectra such as these were readily reproduced with different crystals typically having a mass of about 1 mg. For $\phi = 180°$, one of the hexagonal crystal faces (parallel to a channel direction) is normal to $\mathbf{H}_0$. Rotation studies necessarily show 180° periodicity and the goniometer angle is typically varied in the range of $0° \le \phi \le 180°$ as was done here. However, for rotation about the c axis, the data directly show 60° periodicity as well (note the similarity between the 180° and 124° spectra) and thus only spectra with goniometer angles in the range of 180° and 124° are shown here. The 60° periodicity clearly results from 6-fold symmetry of ferrocene orientations about the c axis. The overall complexity of the spectra immediately indicates that ferrocene adopts a variety of stationary orientations in the thiourea host lattice. Several important features of these spectra, in addition to the 6-fold symmetry, provide the

(20) Wittebort, R. J.; Usha, M. G.; Ruben, D. J.; Wemmer, D. E.; Pines, A. *J. Am. Chem. Soc.* **1988**, *110*, 5668–5671.
(21) (a) Clement, R.; Mazieres, C.; Guibe, L. *J. Solid State Chem.* **1972**, *5*, 436. (b) Clement, R.; Gourdji, M.; Guibe, L. *J. Magn. Reson.* **1975**, *20*, 345.
(22) (a) Heaton, N. J.; Vold, R. L.; Vold, R. R. *J. Am. Chem. Soc.* **1989**, *111*, 3211–3217. (b) Heaton, N. J.; Vold, R. L.; Vold, R. R. *J. Magn. Reson.* In press.

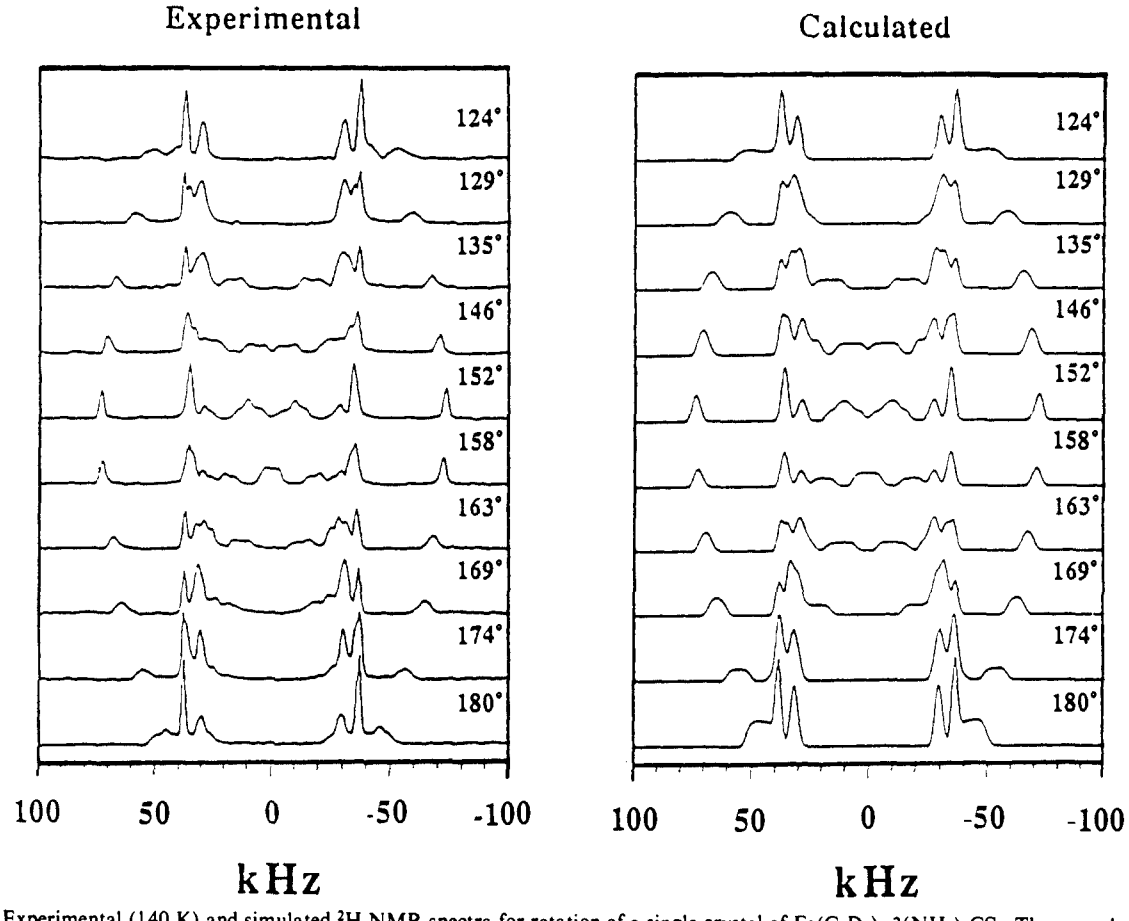

Figure 10. Experimental (140 K) and simulated ^2H NMR spectra for rotation of a single crystal of $Fe(C_5D_5)_2 \cdot 3(NH_2)_2CS$. The crystal was mounted with the needle axis of the crystal perpendicular to the applied field $\mathbf{H}_0$. The crystal was rotated about the needle axis through a series of angles listed on the spectra. Spectra were simulated as described in the text. In each simulation the perpendicular signals were given disorder widths of $\Delta\theta = 20°$ and $\Delta\phi = 7°$, whereas the parallel signals were given disorder widths of $\Delta\theta = \Delta\phi = 3°$. It was found that the parallel orientations lie ~17° off the channel axis.

key to their interpretation. First, in the range of goniometer angles shown, one doublet with large splitting is clearly resolved and passes through the maximum possible frequency of ±73 kHz at $\phi = 150°$. At this setting, the ferrocene molecules contributing to this peak are parallel to $\mathbf{H}_0$ and more generally, in order to pass through the maximum frequency, the molecular axes must lie in a plane perpendicular to the goniometer rotation axis, i.e., the channel axis. The same pattern is repeated with maxima at $\phi = 90°$ and 30° (not shown). We thus observe three distinguishable ferrocene orientations in which the molecular axes are approximately perpendicular to the channel axis and pointing at the hexagonal corners.

The "perpendicular" orientations that contribute lines passing through ±73 kHz at $\phi = 90°$ and 30° give rise to resolved but surprisingly broad peaks in the central part of the spectra in the range of $\phi = 163°$ to 140° in Figure 10. In this range of settings, the lines from perpendicular orientations are much broader than at other settings where the splittings are large. This feature of orientation dependent line width arises from static disorder. As the crystal is rotated, the frequency changes in accordance with eq 3. The frequencies, $\pm\nu$, are largest in magnitude when the molecular axis is parallel to $\mathbf{H}_0$, but the rate at which they change with orientation, $d\nu/d\Omega$, is largest when the molecular axis is at the magic angle relative to $\mathbf{H}_0$ and the splitting is the smallest. Thus, when there is static disorder in molecular orientation ($d\Omega$ is nonzero for a given crystal setting) the resulting line broadening is most noticeable when the splitting is smallest and vice versa as was observed here. A realistic description of the ferrocene molecular orientations must take into account static disorder.

The spectral lines in Figure 10 not accounted for by the "perpendicular" orientations are those that show only small frequency shifts from ±37 kHz (half the maximum) as the sample is rotated about the c axis. These ferrocene orientations lie close to the channel axis. Direct spectral simulation indicates that there are again three distinguishable "parallel" orientations that lie about 17° off the c axis and, as with the "perpendicular" orientations, point at the hexagonal corners of the channel. The "parallel" and "perpendicular" orientations are well-resolved in the 152° spectrum of Figure 10 and direct integration shows that the "perpendicular" orientations are somewhat favored in population by a ratio of 0.55 to 0.45, in good agreement with the Mössbauer results.

The orientational ordering described above can now be used to simulate the entire spectrum for rotation about the c axis as well as for rotation about an axis orthogonal to the channel axis. For a simple picture of the static disorder, we assume that each orientation is characterized by polar and azimuthal disorders, $\Delta\theta$ and $\Delta\phi$, respectively, and that for an average molecular orientation, (θ,ϕ), the molecular direction is equally distributed among all orientations from $(\theta - {}^1/_2\Delta\theta, \phi - {}^1/_2\Delta\phi)$ to $(\theta + {}^1/_2\Delta\theta, \phi + {}^1/_2\Delta\phi)$. The simulation procedure is described elsewhere.[23] Figure 11 demonstrates the procedure for two spectra where the connection of experimental spectrum to the "parallel" and "perpendicular" orientations as well as the disorder widths is readily apparent. In Figure 11A the three doublets arising from the three "perpendicular" orientations and in Figure 11B the two doublets for the three "parallel" orientations are shown for the 159° setting of the c-axis rotation. Figure 11C shows the sum of traces A and B with disorder widths of $\Delta\theta = 20°$ and $\Delta\phi = 7°$ for the "perpendicular" orientations and 3° for both $\Delta\theta$ and $\Delta\phi$ of the "parallel" orientations. The same parameters are used in Figure 11E–H for synthesis of the 78° setting spectrum obtained for rotation about the perpendicular axis. Note in Figure 11F that the parallel orientations, since they are assumed to lie 17° off the

(23) Lowery, M. D. Ph.D. Dissertation, University of Illinois, 1989.

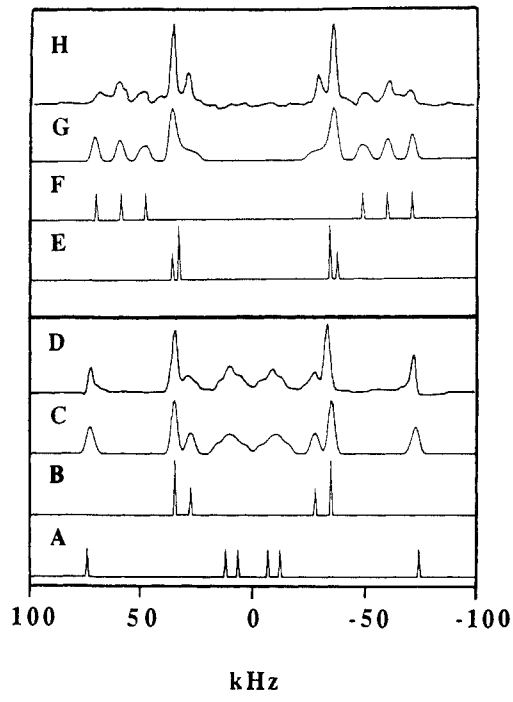

Figure 11. Sample ^2H NMR spectra that show how the disorder model is used to simulate the experimental spectra are illustrated. Traces A–D are for the 159° setting of the *c*-axis rotation profile (crystal axis is perpendicular to the applied field). Traces A and B give line spectra for the three perpendicular orientations and three parallel orientations the ferrocene molecules can adopt, respectively. Trace C is obtained by combining traces A and B including the disorder widths discussed in the text for each of the two types of sites. Trace D gives the experimental 152° setting spectrum. Traces E–H show how the simulated spectrum is constructed for an advantageous orientation of a crystal that is aligned with its *c* axis parallel to the applied field (the 79° spectrum) for the rotational study shown in Figure 12A). The disorder widths (i.e., $\Delta\theta$'s and $\Delta\phi$'s) used in trace E are the same as those used for the simulation in trace C.

channel axis, are resolved into three doublets, which is clearly displayed in the experimental spectrum, see Figure 11H. Full simulations of the *c*-axis rotation are shown in Figure 10, and the experimental and simulated spectra for rotation about an orthogonal axis are shown in Figure 12. The picture used here for static disorder readily accounts for the single-crystal spectra (Figures 10–12) which show surprisingly wide lines. The large polar disorder for the "perpendicular" orientations indicates that the orienting potential for ferrocenes lying perpendicular to the thiourea channel has a weak angular dependence.

To investigate the ferrocene dynamics more directly, spectra of two advantageous crystal orientations were examined as a function of temperature. In Figure 13, spectra are illustrated that were obtained with the channel axis parallel to $\mathbf{H}_0$ (the same setting as the 90° orientation of Figure 12). In this setting, only those motions that change the angle between the ferrocene molecular axis and the channel axis are observed. Reorientation about the *c* axis, such as by exchange among "perpendicular" or among "parallel" sites, has no spectral effect since all orientations have approximately the same frequency, ±37 or ±73 kHz, respectively. At 289 K, a single quadrupole doublet is observed with 4.0 kHz splitting that is reduced to 2.0 kHz if the crystal is rotated by 90° (see Figure 14). Thus, all ferrocene molecules are dynamically equivalent with a residual quadrupole moment axially symmetric about the channel axis and, compared to the low-temperature phase, reduced by a factor of 0.055, the uniaxial order parameter. Spectral resolution is lost as the temperature is lowered below the highest temperature small heat capacity bump at 220 K (ΔH_{trans} = 0.057 kJ/mol), indicating a dramatic slowing of at least some aspects of the rapid ($\tau_c < 10^{-6}$ s) and nearly isotropic dynamics seen at temperatures above 220 K. The ±37 kHz doublet, arising from the low-temperature "perpendicular" orientations, is recovered to a substantial degree when the temperature is lowered to 200 K, whereas the ±74 kHz doublet, identifying the "parallel" orientations, is not easily seen until a lower temperature of 180 K is reached. From this crystal orientation we readily see that the predominant changes in the spectra occur at temperatures above 180 K, i.e., at temperatures higher than the dominant entropy gain. These changes are necessarily due to dynamics that change the angle between the ferrocene molecule and channel axes, such as for exchange between the "parallel" and "perpendicular" orientations.

Spectra obtained with the channel axis orthogonal to $\mathbf{H}_0$ are given in Figure 14. For this setting, reorientation of the molecular axes about the channel direction will affect the spectrum and the 200 K spectrum bears no resemblance to the 150 K spectra as in Figure 13. Thus, as the temperature is raised above the first-order phase transition at 160 K, the "perpendicular" orientations, although largely fixed in the plane, must reorient about the channel axis. This can also occur for the "parallel" orientations.

Concluding Comments

At the outset it should be noted that phase transitions associated with ferrocene have been studied[24] for several years. The thermodynamic properties of ferrocene were first studied in 1960.[24a] A λ-type phase transition at 163.9 K from a low-temperature triclinic phase to a monoclinic high temperature was believed to be present for several years. This well-known λ-type transition was, however, revealed to take place between two metastable phases by Ogasahara et al.[25] in 1979. The stable low-temperature phase was soon found to belong to an orthorhombic system.[26] In addition, ferrocene is known to exhibit an interesting crystal-disintegration below the λ-point, which is an independent phenomenon from the λ-type phase transition. These characteristic features of the ferrocene crystal probably have their origin in the uncommon 5-fold molecular symmetry. Molecules with such a symmetry are hard pressed to settle in a crystal lattice while keeping a long-range periodicity. Such "incommensurability" should also be encountered in the thiourea channel inclusion compound $Fe(C_5H_5)_2{\cdot}3(NH_2)_2CS$.[14]

^2H NMR spectroscopy has been used to characterize definitively the static orientations of ferrocene in the channels of the thiourea inclusion compound $Fe(C_5D_5)_2{\cdot}3(NH_2)_2CS$ below the first-order phase transition at 160.6 K. In the hexagonal channel formed by the thiourea matrix there are six different ferrocene orientations. Three (reduced from six due to the head-to-tail symmetry of ferrocene) are related by a C_3 axis and have the ferrocene molecular axis lying on average perpendicular to that axis. Approximately 55% of the ferrocenes are so oriented at 140 K. The other three orientations also related to each other by the 3-fold symmetry have the ferrocene molecular axis ~17° off the channel axis. For each of these two types of orientations (perpendicular and parallel) there is about each site a static ($\tau_c > 10^{-3}$ s) distribution in orientations characterized by polar ($\Delta\theta$) and azimuthal ($\Delta\phi$) disorders. The large polar disorder ($\Delta\theta$ = 20°) for each of three perpendicular orientations indicates that the orienting potential for the perpendicular ferrocenes about the channel axis is weak. The immediate consequence of this is that the lowest temperature dynamics of the guest molecules, ring rotation aside, is reorientation about the channel axis of the perpendicularly oriented ferrocenes.

Variable-temperature ^2H NMR data for $Fe(C_5H_5)_2{\cdot}3(ND_2)_2CS$ show that, aside from rapid small-amplitude libration at the higher temperatures, the thiourea molecules forming the channels are stationary from 140 to 298 K. The 295 K X-ray structure[13] shows that the molecular planes of the thiourea molecules containing all atoms except H form the faces of the hexagonal channels. The single-crystal NMR results at all temperatures show the DND

(24) (a) Edwards, J. W.; Kington, G. L.; Mason, R. *Trans. Faraday Soc.* **1960**, *56*, 660. (b) Seiler, P.; Dunitz, J. D. *Acta Crystallogr., Sect. B* **1979**, *35*, 457 and references therein.

(25) Ogasahara, K.; Sorai, M.; Suga, H. *Mol. Cryst. Liq. Cryst.* **1981**, *71*, 189.

(26) Seiler, P.; Dunitz, J. D. *Acta Crystallogr., Sect. B* **1982**, *38*, 1741.

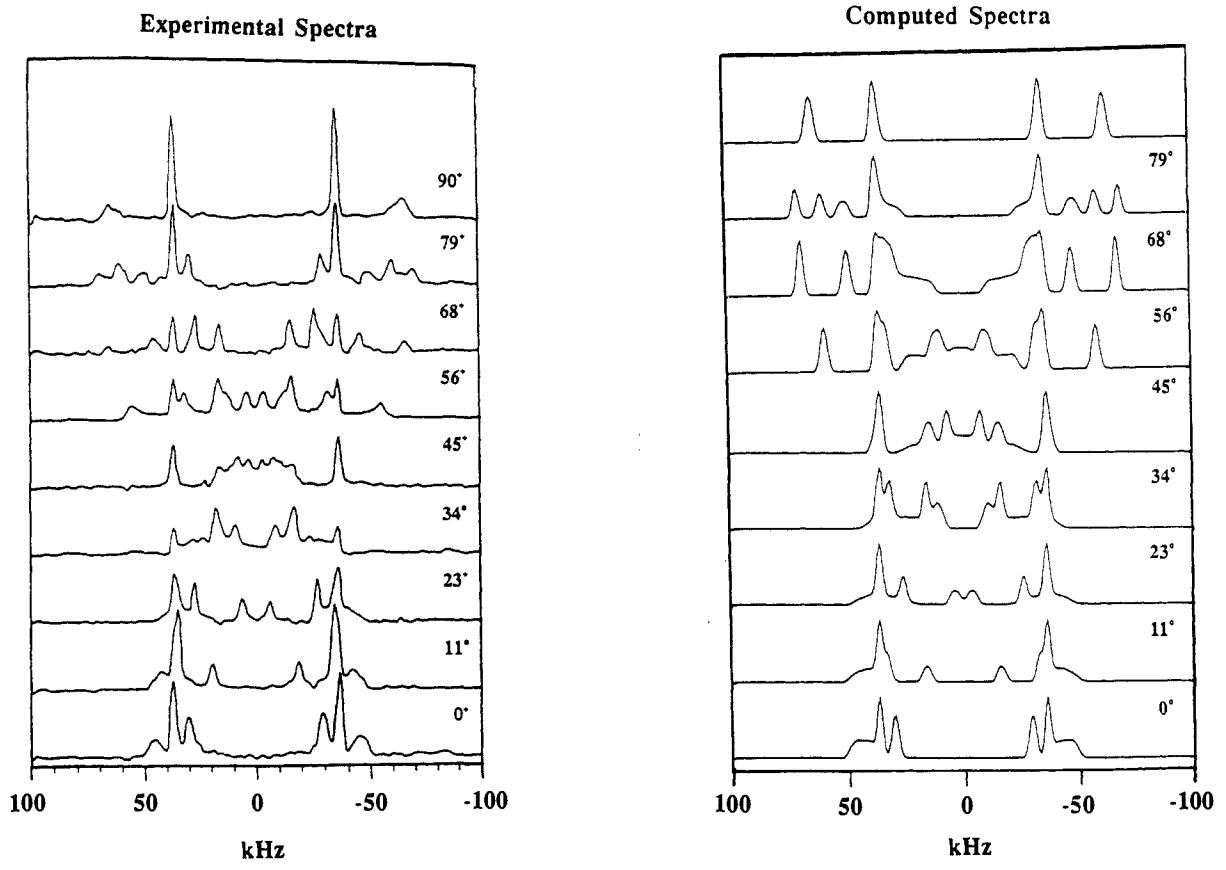

Figure 12. Experimental (140 K) and simulated ^2H NMR spectra for rotation of a single crystal of $Fe(C_5D_5)_2 \cdot 3(NH_2)_2CS$. The crystal was mounted with the needle axis of the crystal perpendicular to the rotation axis and initially parallel to the applied field. The crystal was rotated through a series of angles as listed for each spectrum. Spectra were simulated as described in the text. In each simulation the perpendicular signals were given disorder widths of $\Delta\theta = 20°$ and $\Delta\phi = 70°$, whereas the parallel signals were given disorder widths of $\Delta\theta = \Delta\phi = 3°$.

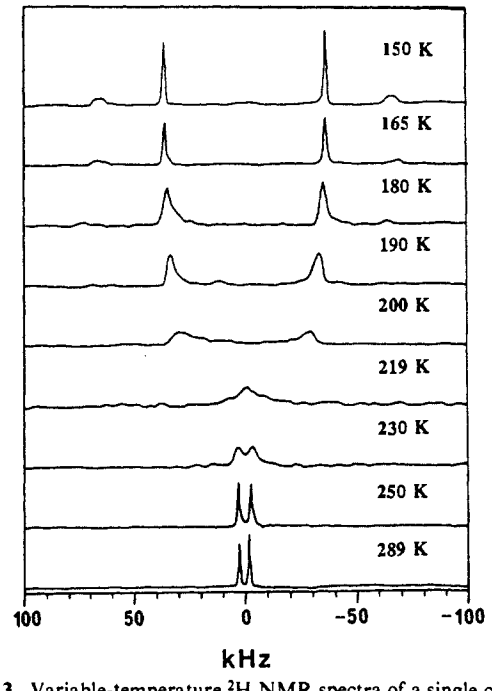

Figure 13. Variable-temperature ^2H NMR spectra of a single crystal of $Fe(C_5D_5)_2 \cdot 3(NH_2)_2CS$. The needle axis of the crystal is parallel to the applied magnetic field.

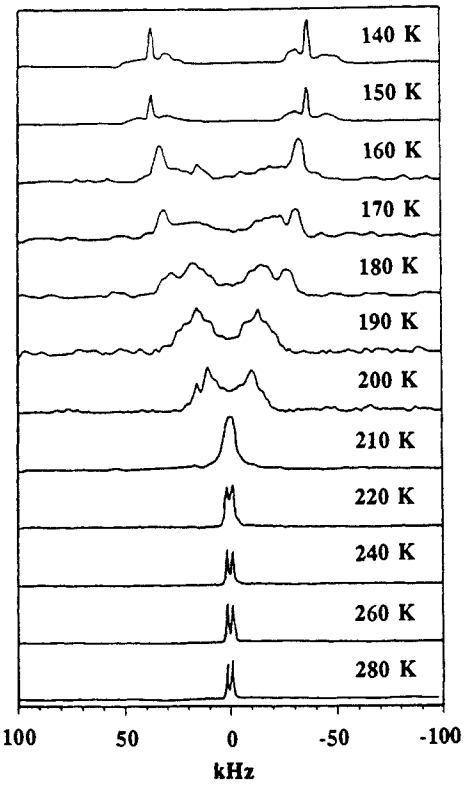

Figure 14. Variable-temperature ^2H NMR spectra of a single crystal of $Fe(C_5D_5)_2 \cdot 3(NH_2)_2CS$. The needle axis of the crystal is perpendicular to the applied magnetic field.

planes are normal to the hexagonal faces. Thus the N–D bonds are directed into the channels and likely interact sterically with the guest.

^2H NMR and ^{57}Fe Mössbauer results for polycrystalline and single-crystal samples of $Fe(C_5D_5)_2 \cdot 3(NH_2)_2CS$ indicate that an increase in the temperature above that of the main first-order phase transition at ~160.6 K leads to the onset of motion of the ferrocene molecules in the channel. Abruptly at ~160 K a second

doublet with reduced quadrupole splitting appears in the Mössbauer spectrum, in addition to the low-temperature doublet for static ferrocenes. This second doublet is associated with ferrocene molecules that are dynamic in the plane perpendicular to the channel axis. The absence of line broadening and relatively little loss in spectral intensity in the Mössbauer spectra in the 160–210 K region leads to the conclusion that the rate of interconversion of ferrocene molecules between parallel and perpendicular orientations is slower than the ^{57}Fe Mössbauer technique can sense, i.e., less than $\sim 10^7$ s^{-1}. This is interesting for an analysis of Mössbauer spectra also shows that the percentage of static ferrocenes oriented parallel to the channel axis decreases from ~34% at 160 K to ~8.7% at 210 K.

By ~221 K the ^{2}H NMR spectrum indicates a rapid almost isotropic tumbling of the ferrocene molecules. In the 220–300 K range the Mössbauer spectrum changes such that it looks like the two doublets coalesce to one very broad doublet and then by ~300 K there is only one Lorentzian remaining with a relatively normal line width. It appears that the rate of the averaging process goes through the window of the ^{57}Fe Mössbauer technique. It is possible that this is the rate at which ferrocenes are exchanging between parallel and perpendicular orientations. If this is the case, this rate would be less than $\sim 10^5$ s^{-1} (^{2}H NMR) in the 160–180 K range and suddenly moves through the Mössbauer window of 10^6–10^9 s^{-1} in the 220–300 K range.

A model that potentially accounts for the above orientations is to assume that the onset of dynamics in the linear arrays of guest molecules arises from the propagation of distinct lattice domains along the channel, i.e., solitons. It is proposed that a soliton disturbance propagates nondispersively through low-dimensional solids with phase velocity approaching the speed of sound. As the soliton propagates, this lattice disturbance can induce transitions between the parallel and perpendicular settings. If the phase velocity is such that the domain walls pass through a thiourea molecule at a rate well in excess of the Mössbauer time scale, 10^7 s^{-1}, then the transition will appear as a discrete jump-like process as we have observed here. The density of soliton excitations is expected to increase with temperature. The density must, however, remain sufficiently low in the temperature range of 160–210 K such that the number of transitions per unit time per guest molecule is less than 10^5 s^{-1} in order that the Mössbauer spectrum show resolved doublets for the parallel and perpendicular setting.

Finally, a few comments about the heat capacity results are in order. In the lowest temperature phase all ferrocene molecules are static. There are six different orientations. In the highest temperature phase all ferrocene molecules are dynamically equivalent and display large-amplitude reorientation of their molecular axes that is symmetric about the channel axis. A simple view of the high-temperature disorder is to assume that the molecules reorient among the six distinguishable orientations identified in the lowest temperature phase. This would give a total transition entropy gain of R ln 6.

The observed high-temperature-order parameter is 0.055, as obtained from the residual ^{2}H quadrupole splitting. This order parameter is predicted exactly if the parallel orientations are assumed to lie 18° off the hexagonal axis and the ratio of parallel to perpendicular populations is 0.42:0.58; both of these are within experimental error of the values determined. Assuming that the parallel orientations are more nearly parallel to the hexagonal axis or that the populations in the parallel and perpendicular sites are more nearly equal substantially increases the order parameter over that observed. Thus, we suspect that at high temperature, as in the low-temperature phase, it is difficult to have neighboring ferrocene molecules oriented parallel to the channel axis. There is probably a cooperativity in the sense that two ferrocenes in neighboring lattice sites cannot simultaneously be both oriented along (ie., 17° off) the channel axis. Such a correlated motion of neighboring ferrocenes can reduce the entropy gain considerably from the simple expectation of R ln 6. A value of $\Delta S = R$ ln 6 is only obtainable if each ferrocene can adopt any of the six distinguishable orientations independent of its neighbor's orientation. The observed value of $\sim R$ ln 4 may indicate that in the complete transformation from static to dynamic for ferrocenes in $Fe(C_5H_5)_2 \cdot 3(NH_2)_2CS$ there is appreciable correlated motion of ferrocenes along the channel axis. Indeed, the lowest temperature heat capacity peaks at 145 and 160 K show the dominant entropy gain, just less than R ln 4, and according to our observations correspond to the abrupt onset of motion of ferrocene molecules in the plane perpendicular to the channel axis. An entropy gain of R ln 3 would be expected if in the 145–160 K region the perpendicular ferrocenes jump between three sites and, as well, the parallel ferrocenes begin to jump between their three positions which are each ~17° off the channel axis.

The additional very small entropy gain associated with the small C_p anomalies seen at ~171, ~186, and 220 K, which occur in a region where large changes are noted in the NMR and Mössbauer spectra, probably reflects the highly correlated nature of interchanges of ferrocenes between parallel and perpendicular orientations. If solitonic disturbances are present, then correlated motion may be a natural consequence.

Acknowledgment. We are grateful for support from National Institutes of Health Grant HL13652 (D.N.H.) and National Science Foundation Grant DMB 8606358 (R.J.W.).